Soft Matter

PAPER

View Article Online
View Journal | View Issue

Cite this: *Soft Matter*, 2025, **21**, 2480

Preparation of hybrid β-chitosan – squid pen protein hydrogel beads by ionic liquid regeneration for adsorption of copper(II) and zinc(II) from wastewater†

Liyan Moralez, Pedro Nakasu * and Jason Hallett *

This study explores the use of squid pen protein to enhance the chemical stability and heavy metal ion (Cu^{2+} and Zn^{2+}) affinity of β-chitosan. Hydrogel beads with enhanced porosity and scalability were prepared using 1-butyl-3-methylimidazolium acetate, ([BMIM][OAc]), which simultaneously functionalized β-chitosan by decreasing its crystallinity and enhancing binding site access, as indicated by Fourier transform infrared (FT-IR) spectroscopy, which revealed intensification of functional group expression. Notably, this functionalization compensated for the effects of glutaraldehyde crosslinking. However, initial experiments noted a reduction in adsorption capacity as the squid pen protein content increased, with Cu^{2+} and Zn^{2+} adsorption being particularly inhibited at lower pH levels due to protonation. Subsequent batch adsorption studies identified optimal conditions for Cu^{2+} and Zn^{2+} uptake, with 24-hours being adequate to appraoch equilibrium, and revealed that adsorption followed pseudo-second-order kinetics, indicative of chemisorption. Furthermore, analysis of adsorption kinetics by intraparticle diffusion revealed that mass transfer was rate-limiting, with Cu^{2+} and Zn^{2+} transport being a multi-step process involving successive and slower phases controlled by external diffusion, intraparticle diffusion and equilibrium, respectively. Lastly, equilibrium studies revealed that the adsorption of Cu^{2+} and Zn^{2+} corresponded with the Langmuir model, suggesting monolayer coverage with maximum adsorption capacities of 67.4 mg g^{-1} for Cu^{2+} and 24.1 mg g^{-1} for Zn^{2+}. Overall, the potential of squid pen protein as an economical filler for β-chitosan-based adsorbents was validated alongside the efficiency of using [BMIM][OAc] for the non-toxic functionalization of β-chitosan. Support of green chemistry principles was evidenced by a high atom economy and low environmental impact, indicating a sustainable method for preparing effective biosorbents.

Received 4th November 2024,
Accepted 23rd February 2025

DOI: 10.1039/d4sm01300j

rsc.li/soft-matter-journal

Introduction

Heavy metal ions are a significant class of pollutants.[1] Incidents of carcinogenic, mutagenic and neurotoxic effects on humans have been attributed to certain species.[2] The danger posed by heavy metal ions is exemplified by their potency at innocuous concentrations, high mobility and longevity in organisms due to bioaccumulation.[3] Heavy metals of high priority include copper (Cu^{2+}), cadmium (Cd^{2+}) and zinc (Zn^{2+}).[1]

Adsorption is a promising strategy for the cost-effective and energy-efficient treatment of dilute effluents, particularly given the diversity of surface functional groups available on different adsorbents, which allows for treatment of a diverse range of effluents, including heavy metal ions.[4] Additionally, minimum waste is produced due to regeneration and recycling of adsorbent. However, conventional carbon- and mineral-based adsorbents are limited by complex synthesis methods and susceptibility to severe loss of efficiency after only a few regeneration cycles, respectively.[5] Moreover, traditional powdered adsorbents are infeasible for commercial adoption due to the economic and time constraints of post-treatment separation and recovery, which typically involve precipitation, centrifugation and filtration.[6]

The poor economic robustness of traditional adsorbents has invigorated interest in cost-effective alternatives, particularly biosorbents. Among biosorbents, biochar has gained significant attention due to its cost-effective synthesis from a wide range of waste biomass residues.[7,8] Biochar's prevalence is further supported by high surface area, microporosity and stability. However, the application of biochar in the removal of heavy metal ions from wastewater has been limited by relatively low removal efficiencies.[7,9] As a result, ongoing efforts are focused on surface modification of biochar through

Dept. of Chemical Engineering, Imperial College London, South Kensington SW7-2AZ, London, UK. E-mail: pedronakasu@gmail.com, j.hallett@imperial.ac.uk

† Electronic supplementary information (ESI) available. See DOI: https://doi.org/10.1039/d4sm01300j

functionalization, chemical grafting and impregnation.[10] However, secondary pollution from these modifications significantly hinders biochar's application in heavy metal ion removal.[7,9]

In contrast, chitosan, the *N*-deacetylated derivative of chitin, is promising due to its biodegradability, biocompatibility, cost-effectiveness and high capacity for heavy metal ion uptake.[3,11] Specifically, β-chitosan, the morphological variant possessing parallel arrangement of adjacent polymer chains, has garnered significant attention.[12] This is due to the more simple extraction of β-chitin from squid waste compared to that of α-chitin from crustaceans. Extraction of β-chitin is less resource-intensive due to squid pens being almost entirely β-chitin and proteins at 49.0% and 46.23%, respectively.[13] Moreover, β-chitin is more soluble and reactive than α-chitin, resulting in more efficient deacetylation.[12] However, the progression of chitosan towards utilization in commercial applications has been hindered by low mechanical strength, substantial cost, limited access to binding sites and inadequate chemical stability in acidic media.[14]

The preparation of spherical hydrogel beads from chitosan is a common modification for increasing porosity, surface area and access to internal binding sites.[14,15] Spherical beads also address the operational limitations associated with powdered or non-structured adsorbents.[16] Notably, their hydrodynamic behaviour and regular packing enable efficient scale-up under low-pressure conditions in continuous-flow fixed-bed column configurations. In comparison, emerging technologies such as magnetic nanoparticles (MNPs) and two-dimensional material-based (2DM-based) adsorbents, with superior specific surface area, require significant optimisation before scale-up, making them less suitable for immediate practical application.[6,17,18] In the case of MNPs, their magnetic nature facilitates recovery from solution but their small size requires fluidized bed or in-series stirred tank configurations.[17] Moreover, aggregation remains a major challenge during recovery using high-gradient magnetic separators. Meanwhile, for 2DM-based adsorbents there exists a need for microstructure design and optimisation.[6]

Chemical crosslinking is the primary strategy for enhancing the stability of chitosan in acidic media. Polymeric networks, with enhanced acidic resistance, are prepared by exploiting the ability of bifunctional crosslinkers to covalently bridge chitosan chains at amine or hydroxyl sites.[12] The preservation of hydrogel structure in acidic media allows for regeneration. However, most crosslinkers are toxic and impart impaired mass transfer as well as brittleness.[14] The affinity of crosslinkers towards amine groups is an additional challenge, resulting in reduced negative surface charge and adsorption capacity. Currently the most reliable and utilized crosslinker is glutaraldehyde, which targets amine sites by imine (Schiff) bond formation.[12]

Ionic liquids (ILs) are compounds, comprised of anions and cations, with melting points not exceeding 100 °C. IL treatment or solubilization is a novel strategy for functionalizing chitosan. This method functions by reducing the crystallinity of chitosan through the rearrangement of chitosan's linear chains.[15,19] The disruption of inter- and intra-molecular bonds in the amorphous and crystalline regions of chitosan occurs due to the anions of ILs possessing high hydrogen bond accepting abilities, which effectively enable the formation of hydrogen bonds with amine and hydroxyl groups.[20] The merit of IL solubilization as a novel synthesis strategy is supported by the limited uptake of metal ions by chitosan's crystalline planes, with chelation occurring exclusively on the amorphous regions.[21]

IL treatment is operationally simple. It resembles the phase separation method for bead preparation using dilute organic acids. The key difference is regeneration in ethanol or water *via* an antisolvent mechanism rather than neutralization in alkaline media.[19,22] This is advantageous as it enables solvent recycling. IL systems also benefit from good thermal stability, low vapour pressure and cosolvent compatibility.[20]

1-Butyl-3-methylimidazolium acetate ([BMIM][OAc]) is the IL reported to have the highest solvating ability for chitosan with a maximum loading capacity of 8.40% at 100 °C.[20] Moreover, the FT-IR spectrum of chitosan regenerated from [BMIM][OAc] is not indicative of side reactions or the production of ammonium salts, with the primary structure remaining unaltered. However, [BMIM][OAc] is very viscous with dimethyl sulfoxide commonly used as a cosolvent to facilitate extrusion.[22] Lastly, like other ILs, [BMIM][OAc] has been reported in previous work to impart poor mechanical properties on regenerated chitosan beads.[23]

Interpenetrative blending facilitates augmenting chitosan's mechanical strength beyond recasting and has been coupled with IL solubilization to compensate for enhanced brittleness. Interpenetrated polymer networks (IPNs) are comprised of two or more polymers, which have undergone molecular interlacing through diffusion prior to being chemically crosslinked.[24] IPN formulations are noteworthy for their idiosyncratic properties, which can be tuned by altering the co-polymer dosage. In this regard, hybrid chitosan-based IPNs with enhanced chemical stability, mechanical properties and adsorption capacities have been reported.[12] The influence of co-polymers on adsorption arises from their contribution to functional group diversity and density, with lower pK_a values conferring higher negative surface charge.[12] Polysaccharides and proteins are promising blend polymers due to their hydroxyl, sulfhydryl, amine and carboxyl content.

Squid pen (SP) protein, extracted from β-chitin, is postulated to have a high diversity and density of functional groups. The mechanical strength of squid pens, the corresponding biomass, provides motivation for suitability as a co-polymer on the basis that β-chitosan and SP protein hybrid materials can be reverse-engineered to have similar properties. Furthermore, SP protein is an underutilized byproduct of β-chitosan production. As such, its inclusion affords a valuable opportunity to optimize the β-chitosan value chain and reduce the cost of a hybrid biosorbent. Partially substituting β-chitosan with SP protein, a starting material, also reduces the environmental footprint of a hybrid biosorbent since chitin deacetylation occurs at 100–160 °C over several hours and requires 40–50% sodium hydroxide.[12]

This study focused on synthesizing highly functionalized and physically enhanced hybrid biosorbents from β-chitosan and SP protein for removing Cu^{2+} and Zn^{2+} from heavily contaminated industrial wastewater. To the best of our knowledge, similar IPN formulations have not been reported for adsorption or any other capacity. Recasting from [BMIM]

[OAc] was employed to facilitate co-polymer interlacing, confer physical modification into spherical beads, enable non-toxic functionalization and promote green chemistry through solvent recycling. The hybrid biosorbent beads were characterized using optical microscopy and Fourier transform infrared (FT-IR) spectroscopy to assess their structural properties and identify functional groups. Lastly, batch adsorption studies were performed in successive stages to assess the contribution of SP protein content and optimize Cu^{2+} and Zn^{2+} removal by investigating the effects of solution pH, agitation period and initial solution concentration.

Experimental

Chemicals and materials

β-chitosan (~580 000 Da) was purchased from Glentham Life Sciences. The degree of deacetylation was 92% as determined by nuclear magnetic resonance (NMR) using a JNM-ECZL 400S spectrometer (JEOL). Sieved squid pen was sourced locally and determined to have a moisture content of 5% after overnight drying at 105 °C. Sodium hydroxide pellets (NaOH, 98.8%) and absolute ethanol (≥96%) were sourced from VWR Chemicals. 1-Butyl-3-methylimidazolium acetate ([BMIM][OAc]) was sourced from Proionic, with a moisture content of 1.75% as determined on a Karl Fischer C20 Coulometer (Mettler Toledo). Deionized (DI) water (≥18 MΩ) was obtained from a Centra R200 (ELGA LabWater). Glutaraldehyde solution (~50%), dimethyl sulfoxide (DMSO, analytical grade, ≥99.7%), zinc nitrate hexahydrate ($Zn(NO_3)_2{\cdot}6H_2O$, analytical grade, ≥99.0%), and copper(II) sulphate pentahydrate ($CuSO_4{\cdot}5H_2O$, analytical grade, ≥99.0%) were sourced from Sigma-Aldrich. Hydrochloric acid (HCl, ~37%) and nitric acid (HNO_3, ~67–69%) of TraceMetal™ designation were obtained from Fisher Scientific. All chemicals were used without modification and stored as recommended.

Squid pen protein extraction

A slurry comprised of 5% squid pen (dry mass) was prepared by the addition of a suitable volume of 0.5 M NaOH solution. The slurry was stirred at 400 rpm and ambient temperature for 3 hours, then vacuum filtered. Isoelectric precipitation (pH 3.5) was performed on the filtrate by the dropwise addition of 3 M HCl solution. A Jenway 3510 pH Meter (Cole Parmar) was used for all pH-related measurements. The precipitated protein was centrifuged at 3600 rpm for 20 minutes using a VWR Mega Star 3.0 (Avantor). The supernatant was discarded while the protein was washed with DI water 4 times. The washed protein was immersed in liquid nitrogen and freeze dried for 48 hours on a Freezone 6 Litre Benchtop Freeze Dryer (Labconco).

Hydrogel bead preparation

Three types of β-chitosan-SP protein hydrogel beads were studied. These were designated as CH, CH-SQ-25 and CH-SQ-50, with β-chitosan contents of 100%, 75% and 50%, respectively. The remainder of their content consisted of SP protein.

A batch-equivalent of casting solution was prepared from a solvent system comprised of 12 g [BMIM][OAc] and 12 g DMSO, to which β-chitosan and SP protein were added for a total solid loading of 0.6 g (5% IL mass). The proportion of the co-polymers was dependent on the bead type as previously described. The dissolution of the dispersed polymers was achieved through continuous stirring at 400 rpm and 100 °C for 20 hours. Each batch of casting solution was manually extruded into 250 mL of absolute ethanol using an 18-g needle (ID 0.838 mm) paired alongside a 3 mL syringe. During extrusion, the casting solutions were maintained at 100 °C to reduce viscosity and the 18-g needle was replaced upon clogging. The regenerated hydrogel beads were left to cure for 20 hours in absolute ethanol under gentle stirring at 100 rpm. The cured beads were removed from the ethanol-IL mixture by filtration through a Büchner funnel. The filtrate was discarded. However, the [BMIM][OAc] : DMSO = 1 : 1 solvent system was recoverable by rotary evaporation. The recovered beads were washed 3 times. This entailed adding the beads to 250 mL of DI water and stirring at 100 rpm for an hour prior to filtration. The washed beads were transferred to 100 mL of 0.25% glutaraldehyde solution and crosslinked for 20 hours under gentle stirring at 100 rpm. A recovery and washing scheme similar to the one detailed after curing was observed. The crosslinked beads were then immersed in liquid nitrogen and freeze dried for 48 hours using a Freezone 6 Litre Benchtop Freeze Dryer.

Microscopy

The hydrogel beads were observed with a Leica DM2500 (Leica). Their porosity was analysed by pressing a sample bead between glass slides under 4× magnification with light directed from above.

Fourier transform infrared spectroscopy (FT-IR)

The FT-IR spectra of β-chitosan, SP protein, and the hydrogel beads were recorded on an Agilent Cary 630 (Agilent) equipped with a Diamond-ATR sampling module obtained from the same manufacturer. The hydrogel beads were pulverized for analysis but otherwise remained unmodified. The spectral acquisition was performed over the range of 4000–500 cm^{-1} with 32 sample scans at room temperature.

Zeta potential

The mean zeta potentials of β-chitosan and SP protein were determined using a Litesizer 500 (Anton Paar). The polymers were suspended in DI water and loaded into omega cuvettes, from the same manufacturer, for analysis. All measurements were performed at room temperature.

Preparation of synthetic wastewater

Cu^{2+} and Zn^{2+} solutions with concentrations of 50, 100, 150, 200 and 250 ppm were prepared by dissolving the corresponding amounts of either $CuSO_4{\cdot}5H_2O$ or $Zn(NO_3)_2{\cdot}6H_2O$ in DI water.

Adsorption experiments

The adsorption characteristics of the hydrogel bead types were assessed by batch studies involving the addition of hydrated

beads to either copper or zinc wastewater in 50 mL centrifuge tubes. The agitation speed, solution volume, biosorbent mass and metal ion concentration were dependent on the specific experiment as described in the following sections. Each of the various experiments was performed in duplicate. Equipment-wise, all instances of centrifugation and pH measurements were performed on the aforementioned equipment while agitation was provided using a Multi Reax Orbital Shaker (Heidolph).

The metal ion concentration, C_t, in the treated wastewater samples was determined twice by inductively coupled plasma mass spectroscopy on an Agilent 7900 ICP-MS (Agilent). A dilution matrix comprised of 1% HCl and 2% HNO_3 was utilized alongside commercial calibration standards. The removal efficiency, R_e, of heavy metal ions was calculated according to the following equation:

$$R_e = \frac{C_i - C_t}{C_i} \times 100 \quad (1)$$

where C_i is the heavy metal ion concentration (ppm) before treatment.

The amount of heavy metal ions adsorbed per dry mass of biosorbent or adsorption capacity, q_t, in mg g^{-1} was calculated according to the following equation:

$$q_t = \frac{C_i - C_t}{m_{dry}} \times V \quad (2)$$

where V is the volume of the heavy metal ion solution (L) and m_{dry} is the dry mass of the biosorbent (g).

Initial pH studies

Experiments were conducted within the pH range of 2–5 for Cu^{2+} and 3–6 for Zn^{2+}. These ranges were chosen to prevent the precipitation of the insoluble hydroxide complexes of the respective metal ions, as guided by thermodynamic speciation modelling conducted by Albrecht *et al.*[25] The disparity between the ranges reflects the predominance of insoluble $Cu(OH)_2$ at pH levels significantly below 6, even at relatively low concentrations (<10 ppm). For Zn^{2+}, $Zn(OH)_2$ was not reported as the primary specie below pH 7 for the heavy metal ion concentration range proposed for the equilibrium studies. However, estimates based on K_{sp} indicated initial precipitation near pH 7 for the highest concentration (250 ppm), leading to its exclusion from the studies. The unsuitability of the higher pH levels (Cu^{2+} pH > 6, Zn^{2+} pH > 7) was also confirmed during synthetic wastewater preparation and supported by previous work, which reported diminished uptake due to precipitation at those pH levels.[26,27]

To conduct the initial pH studies, a slightly modified protocol proposed by Sutirman *et al.* was used for the experiments.[28] For each batch study, 0.025 g of each bead type were hydrated for 24 hours in 20 mL of DI water. The hydrated beads were filtered to remove excess water prior to being transferred into 12 mL of 100 ppm Cu^{2+} or Zn^{2+} solutions at the various integer pH values within the ranges. An initial pH method was used with the pH value of the solutions not being adjusted during the adsorption period. For consistency, the initial adjustments to the pH value were done on 100 mL aliquots of 100 ppm Cu^{2+} or Zn^{2+} solution from the same stock solution. Solutions of 0.1 M NaOH and 0.1 M HCl were used to perform the initial adjustments. The immersed beads were agitated/treated at 800 rpm for an hour. The treated wastewater solutions were centrifuged at 4000 rpm for 3 minutes, with acceleration and braking levels set at 9. The supernatants were filtered through a 0.2 μm filter for analysis.

Kinetic studies

CH-SQ-25 beads, the hybrid beads with the highest removal efficiency in the pH studies, were utilized to obtain kinetic data. Similarly, the optimum conditions from the previous section were used to maximize adsorption. The experiments were slightly modified from the pH studies. The scale was increased four-fold to enable repeated sampling without vastly altering the solution volume. Firstly, 0.1 g of CH-SQ-25 beads were hydrated for 24 hours in 40 mL of DI water. The hydrated beads were filtered to remove excess water and transferred to 48 mL of 100 ppm Cu^{2+} or Zn^{2+} solution at the optimum pH value (Cu^{2+} pH 5, Zn^{2+} pH 6). The immersed beads were agitated/treated at 1200 rpm. The higher speed reflected the larger scale. A 1 mL syringe was utilized for sample withdrawal at the following time intervals: 30 minutes, 60 minutes, 90 minutes, 3 hours, 6 hours, and 24 hours. The samples were filtered through a 0.2 μm filter for analysis.

Equilibrium studies

CH-SQ-25 beads and optimum conditions were used as stated in the previous section. These experiments closely resembled those performed by Sutirman *et al.*[28] The main difference was the selection of 50–250 ppm as the concentration range based on studies conducted by Wittmer *et al.*[22] This range coincides with typical effluent concentrations for both Cu^{2+} and Zn^{2+} from heavy industrial sources related to primary metal handling, such as mining and smelting, or the intensive use of metals or metal-based chemicals, as seen in electroplating.[29–38] Importantly, these sources are the primary contributors to anthropogenic Cu^{2+} and Zn^{2+} contamination, whereas tanning, textile and urban sources typically do not exceed 15 ppm.[39–45]

For each study, 0.025 g of CH-SQ-25 beads were hydrated for 24 hours in 20 mL of DI water. The hydrated beads were then filtered to remove excess water and transferred to 12 mL of Cu^{2+} or Zn^{2+} solution at the various concentrations and optimum pH value (Cu^{2+} pH 5, Zn^{2+} pH 6). The beads were agitated/treated at 900 rpm for 24 hours. The slightly more intense agitation speed helped prevent settling during the longer period. After 24 hours, the treated wastewater solutions were centrifuged at 4000 rpm for 3 minutes, with acceleration and braking levels set at 9. The supernatant was filtered through a 0.2 μm filter for analysis.

Results and discussion

Physical characterization

Recasting using [BMIM][OAc] proved effective for synthesizing hydrogel beads from β-chitosan and SP protein, as evidenced by

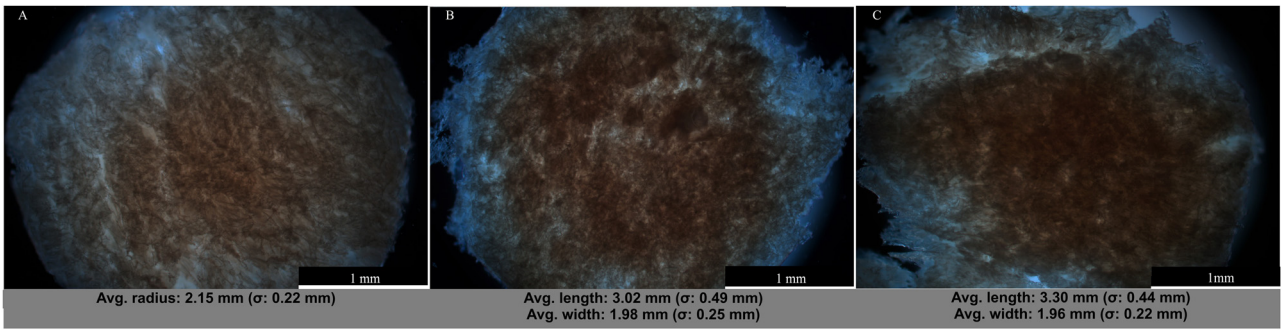

Fig. 1 Average size measurements and optical microscopy at 4× magnification of (A) CH beads, (B) CH-SQ-25 beads and (C) CH-SQ-50 beads.

the different bead types displaying fibrous, highly interwoven porous structures (Fig. 1). However, bead geometry was noted to become less-defined at higher SP protein content. Notably, CH beads were spherical, whereas CH-SQ-25 and CH-SQ-50 beads were ellipsoidal with visible voidage. These transitions in bead shape were further corroborated by size measurements, which revealed an increase in length and decrease in width as SP protein increased. Additionally, all bead types displayed brittleness, though to varying degrees. In this regard, CH-SQ-50 beads were the most fragile, pulverizing when gently pressed.

The non-uniformity and brittleness of CH-SQ-25 and CH-SQ-50 beads may indicate inadequate interlacing of SP protein and β-chitosan functional groups. However, methodological factors must also be taken into account, especially since the physical modification process successfully conferred porosity to all bead types. Importantly, the sphericity and batch uniformity of CH beads highlights the potential for optimizing CH-SQ-25 and CH-SQ-50 recasting, as maintaining constant total solid loading overlooked β-chitosan's larger molecular weight compared to SP protein resulting in significant variation in casting solution viscosity. This is supported by previous studies by Wittmar *et al.*, which explored the influence of casting solution viscosity on the porosity, surface area and shape of β-chitosan-based beads regenerated from ILs.[22] In practice, extrusion from an 18-g needle may have been adequate for the highly viscous casting solution of CH beads but unsuitable for the significantly less viscous casting solutions of CH-SQ-25 and CH-SQ-50 beads.

Other opportunities for optimization were also identified. The brittleness of the CH beads suggests contributions from crosslinking and IL treatment, with the severity of either step influencing the final properties. In fact, the effect of crosslinking was evident in earlier experiments, with the glutaraldehyde concentration maintained relatively low (0.25%) as a deterrent. Regarding IL treatment with [BMIM][OAc], similar observations have been reported by Sun *et al.* for chitosan regeneration from [BMIM][Cl].[19]

Fourier transform infrared (FT-IR) spectra

FT-IR spectral analysis of β-chitosan and SP protein elucidated the chemical and structural derivatives present on the polymer chains (Fig. 2). The spectrum for β-chitosan was consistent with

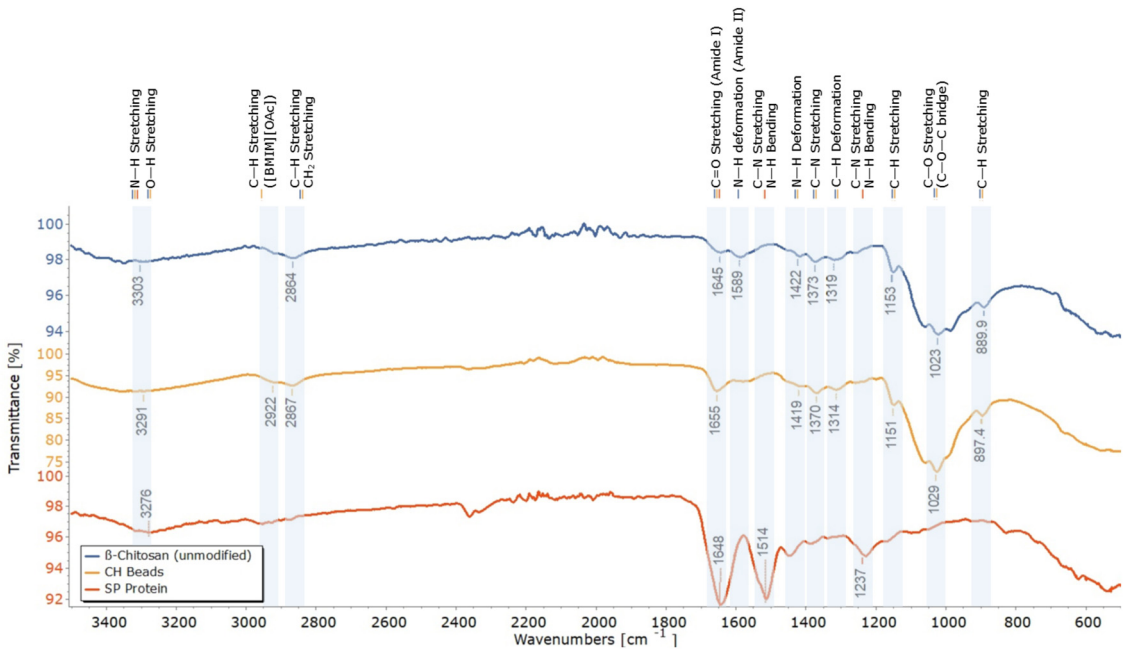

Fig. 2 FT-IR spectra of unmodified β-chitosan, CH beads (100% β-chitosan) regenerated from [BMIM][OAc] and SP protein.

previous studies.[19,20,22,28,46–51] The band at 3303 cm^{-1} related to overlap between N–H and O–H stretching vibrations.[28] The band at 2864 cm^{-1} was allocated to symmetric and asymmetric C–H and CH_2 stretching.[20,28] The bands at 1645 and 1589 cm^{-1} were due to C═O stretching (amide I) of the residual acetamido groups and N–H deformation vibrations of NH_2 groups (amide II), respectively.[28] The band at 1422 cm^{-1} was attributed to N–H deformation vibrations of NH_2 while the band at 1319 cm^{-1} related to C–H deformation. The band at 1373 cm^{-1} was assigned to C–N stretching vibrations.[48] The minor bands at 1153 and 890 cm^{-1} were assigned to C–H stretching.[51] Lastly, the prominent band at 1023 cm^{-1} was characteristic of the C–O stretching vibrations of the C–O–C bridge.[28,48] For SP protein, defining bands relating to secondary structure were observed. The band at 1648 cm^{-1} was assigned to amide I vibrations arising from C═O stretching while the band at 1514 cm^{-1} was the combination of C–N stretching and N–H bending.[52] The amide III band at 1237 cm^{-1} related to C–N stretching and N–H bending. The band at 3276 cm^{-1} indicated O–H stretching.

The spectra of β-chitosan and CH beads were compared to assess the effectiveness of IL treatment in [BMIM][OAc] as a functionalization strategy (Fig. 2). Both spectra exhibited the same bands, with negligible shifting. Notably, the bands at 3291 and 1029 cm^{-1} were considerably more intense for CH beads. This corresponded with the enhanced inter- and intramolecular interactions from the rearrangement of β-chitosan's crystalline planes by the acetate anions.[48] Additionally, the characteristic bands related to ammonium did not decrease in intensity as expected after crosslinking. For reference, decreases in band intensity at 3291, 1655, 1419, 1314 and 1151 cm^{-1} have previously been reported from glutaraldehyde crosslinking.[28,47] The only indication of crosslinking was the disappearance of the band at 1589 cm^{-1} related to N–H bending of NH^2 groups. Lastly, a band indicative of aliphatic C–H stretching vibrations of methyl groups on the [BMIM] cation appeared at 2922 cm^{-1} on the CH beads' spectrum serving as the only evidence of IL treatment and suggesting inefficient curing or washing stages.[53]

Fig. 3(A) illustrates the spectra for the various beads types. Close similarity between the spectra was noted. Notably, no contribution from SP protein was discerned on the spectra for CH-SQ-25 and CH-SQ-50 beads. Additionally, the intensity of the bands at 3291, 2867, 1419, 1370, 1314 and 1029 cm^{-1} decreased as the SP protein content increased, indicating that the SP protein did not enhance the functional group density on the biosorbents, with β-chitosan being the primary contributor.

The 1700–1450 cm^{-1} spectral range offered insight into the absence of discernible bands related to SP protein on the FT-IR spectra for CH-SQ-25 and CH-SQ-50 beads. From Fig. 3(B), it was observed that amide I vibrations were shared by SP protein and CH beads (regenerated β-chitosan) at 1655 and 1648 cm^{-1}, respectively. It is probable that hydrogen bonding among the polymers resulted in the bands for CH beads and SP protein shifting slightly and merging at 1653 cm^{-1} on the spectra of CH-SQ-25 and CH-SQ-50 beads. As for the amide II band present at 1514 cm^{-1} on the spectrum for SP protein, the absence from the spectra of CH-SQ-25 and CH-SQ-50 beads has been attributed to glutaraldehyde crosslinking.

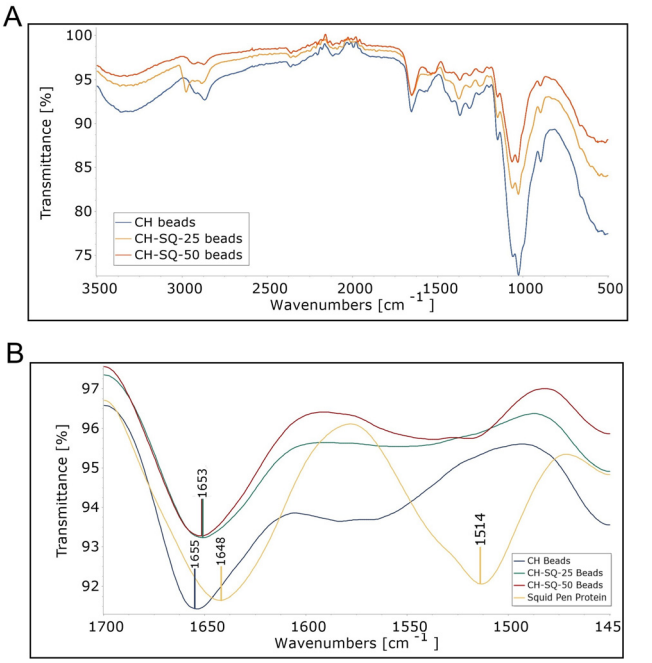

Fig. 3 FT-IR Spectra of CH, CH-SQ-25 and CH-SQ-50 beads showing the effect of SP protein content over (A) 3500–500 cm^{-1} spectral range and (B) 1700–1450 cm^{-1} spectral range with inclusion of SP protein spectrum for comparison.

Influence of pH

The effect of solution pH on the adsorption of heavy metal ions by the different bead types was investigated to understand the influence of surface charge. The determination of an optimum pH value for the subsequent studies was an added objective.

The efficiency of Cu^{2+} removal from a 100-ppm solution by the different beads types was recorded for different pH values after an hour of treatment (Fig. 4(A)). All bead types exhibited a similar pH dependence, with Cu^{2+} uptake increasing sharply over the pH range of 2–3, after which improvements became gradual. Importantly, statistical differences were not noted at higher pH levels (4–5). An optimum pH value of 5 was noted.

The removal of Zn^{2+} by the beads was investigated under identical conditions (Fig. 4(B)). All bead types showcased a similar pH dependence with uptake being relatively low within the pH range of 3–4 before sharply increasing in the range of 4–5. For higher pH values (5–6), the removal efficiency of Zn^{2+} only slightly increased. The results suggested an optimum pH of 6.

The reduced removal efficiencies of Cu^{2+} and Zn^{2+} at lower pH values suggests that the adsorption of heavy metal ions was regulated by the surface charge of the beads, particularly from the protonation of non-crosslinked amine groups.[15] Protonation entails electrostatic repulsion of heavy metal cations and unfavourable adsorption due to competitive occupation of active sites by protons.[15,46] The opposite effect at high pH values is responsible for more favourable adsorption. This was not observed experimentally possibly due to reduced

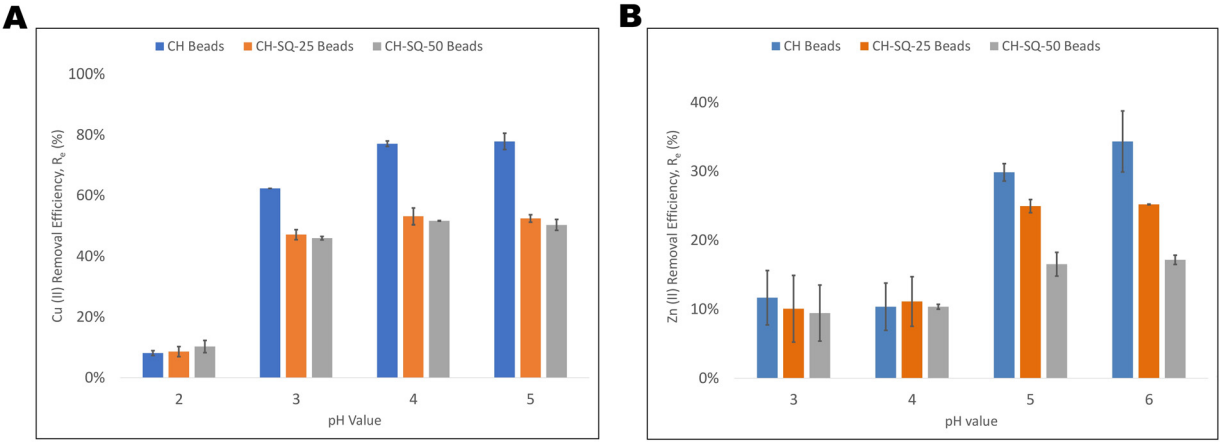

Fig. 4 The effect of solution pH on the removal efficiencies achieved by CH, CH-SQ-25, and CH-SQ-50 beads from 100 ppm heavy metal ion solutions: (A) Cu^{2+} and (B) Zn^{2+}.

sensitivity at higher pH levels. However, it must be noted that the heavy metal ion solutions were unbuffered. Moreover, no adjustments were performed during the agitation period.

Under identical conditions, all bead types exhibited a lower affinity for Zn^{2+}. Previous studies have reported similar results for Zn^{2+} and Cu^{2+} for both single-ion and competitive batch adsorption studies.[54] The consensus is that the adsorption of bivalent heavy metal ions onto chitosan is governed by the Irving–William series, which describes the stability of bivalent transition metal complexes, with Cu^{2+} being the most stable.[55]

Regarding bead type, higher SP protein content negatively affected the removal efficiencies of Zn^{2+} (Fig. 4(B)). For Cu^{2+}, CH beads had a greater affinity. However, the difference in uptake by CH-SQ-25 and CH-SQ-50 beads was small (Fig. 4(A)). The lack of a similar trend for Zn^{2+} may be attributed to a lower affinity for chelation with chitosan. In general, the results suggested that SP protein was not suitable as a functional agent for heavy metal ion adsorption. This finding was consistent with the FT-IR spectra for CH-SQ-25 and CH-SQ-50 beads, which showed a decrease in functionalization at higher SP protein content. The mean zeta potentials, under neutral condition, for SP Protein and β-chitosan of 26.6 mV and 11.6 mV, respectively, offered a supplementary explanation with higher cationic surface charge on SP protein being supportive of greater resistance for the adsorption of Cu^{2+} and Zn^{2+}. Notably, inherently higher cationic surface charge of SP protein may enhance interactions with heavy metal ions that exist as anionic coordination compounds (*e.g.* $HCrO_4^-$ and $PdCl_4^{2-}$), which did not form part of the study.[6]

Lastly, desorption studies were not performed. However, CH and CH-SQ-25 beads maintained their physical form after agitation and recovery. This demonstrated great potential, except for slight vulnerability to acidic conditions, as observed with partial dissolution at pH 2 for the Cu^{2+} studies. For CH-SQ-50 beads, breakage was observed, but the extent was difficult to assess due to non-uniform bead geometry, as previously discussed. Despite this, breakage was deemed minimal, with the release of bead fragments not being problematic, as both co-polymers are biodegradable. Overall, the findings do not discredit SP protein as a filler co-polymer, since it is directly derived from the same biomass as β-chitosan. Moreover, the observed breakage could be addressed by optimising the recasting process to improve uniformity and mechanical integrity, as previously discussed, with this study serving as a proof of concept.

Kinetic studies

Kinetic studies offered insight into the mechanism behind heavy metal ion uptake by CH-SQ-25 beads, while simultaneously examining the suitability of a 24-hour treatment period for reaching equilibrium. The pseudo-first-order (PFO) and pseudo-second-order (PSO) models were used as adsorption reaction models to analyse the nature of the interactions between the biosorbent and heavy metal ions. Additionally, the intraparticle diffusion model was employed for elucidating the mass transport steps involved in the transfer of the heavy metal ions to the adsorption sites on the CH-SQ-25 beads.

Fig. 5(A) illustrates the time-course adsorption of Cu^{2+} by CH-SQ-25 beads from a 100-ppm solution. Equilibrium was gradually approached over the 24-hour treatment period at an adsorption capacity of 40.1 mg g^{-1}. Notably, adsorption was initially rapid as evidenced by the adsorption capacity after 3 hours being 32.8 mg g^{-1} or 83% of the equilibrium value.

The kinetics for Zn^{2+} removal were also studied (Fig. 5(B)). The equilibrium adsorption capacity was 8.3 mg g^{-1} after 24 hours of treatment. Remarkably, this was almost achieved after only 6 hours, at a corresponding adsorption capacity of 8.1 mg g^{-1}. The remainder of the initial treatment period was equally rapid with 6.3 mg g^{-1}, or 76% of the equilibrium value having been adsorbed after 3 hours. Notably, the time-course removal efficiency after 1 hour was 9% as opposed to 25% from the pH studies, which suggests batch variation in the synthesis of the same bead type or scale-up limitations. The discrepancy was not noted for Cu^{2+}, which may indicate that the lower affinity for Zn^{2+} may have been a factor.

The parameters for the PFO and PSO models are given on Table 1. For Cu^{2+}, the PSO model demonstrated a superior fit

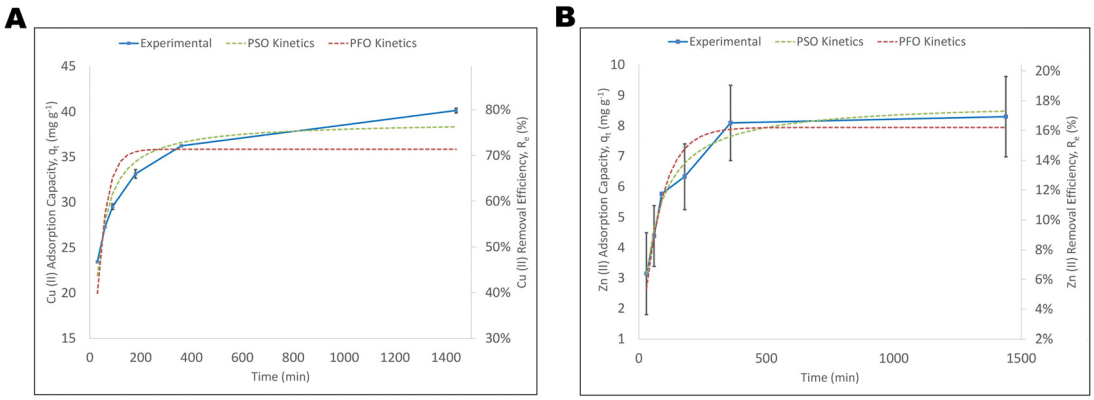

Fig. 5 Reaction kinetic models in terms of adsorption capacity and removal efficiencies for the adsorption by CH-SQ-25 beads from 100 ppm heavy metal ion solution: (A) Cu^{2+} and (B) Zn^{2+}.

with a correlation coefficient, R^2, of 0.9466, compared to 0.7358 for the PFO model. Additionally, the estimate for equilibrium capacity from the PSO model was in reasonable agreement with the experimental value, whereas the value predicted using the PFO model deviated considerably (>10%). In the case of Zn^{2+}, the predicted equilibrium capacities from both models were relatively consistent with the experimental value. Overall, both models provided a good fit, with the PSO model having a slightly better correlation coefficient of 0.9733, compared to 0.9371 for the PFO model. However, the PSO model was more successful in capturing the equilibrium region, making it a more suitable description of the adsorption process. Plotting the PFO and PSO models with the obtained parameters (Fig. 5) visualized the more precise fit provided by the latter model over the entire time domain for both heavy metal ions. Therefore, the PSO model was accepted to describe the adsorption of both Cu^{2+} and Zn^{2+}. This suggested that the adsorption mechanism involved chemisorption or complexation based on the exchange or sharing of electrons between the heavy metal ions and the adsorbent functional groups.[15,28]

Regarding IPD, three independent regions were observed across restricted time domains for the adsorption of both Cu^{2+} and Zn^{2+} (Fig. 6). The distinct regions were identified as 30–90 min, 90–360 min, and 360–1440 min. Additionally, as seen on Table 1 the fitted IPD models exhibited non-zero intercepts, C_{1-3}, for both metal species. Therefore, it was deduced that IPD is not the sole rate controlling process but instead three distinct phenomena control the rate of Cu^{2+} and Zn^{2+} adsorption, with one being rate limiting in any particular region. Nonetheless, a good fit for all regions confirmed that IPD contributed to the adsorption process. This type of multi-step process is consistent with those reported in previous work on porous adsorbents.[50,56–58] The initial region has been postulated to account for film (external) diffusion, describing the transport of Cu^{2+} and Zn^{2+} from the bulk liquid phase to the surface of the CH-SQ-25 beads.[56–59] This process was noted to be the fastest, as indicated by larger IPD rate constants, K_{IPD}. The second region reflects the influence of pore (intraparticle) diffusion, during which Cu^{2+} and Zn^{2+} uptake experiences increased resistance from the porous structure of the CH-SQ-

Table 1 Kinetic parameters for adsorption reaction and intraparticle diffusion models for Cu^{2+} and Zn^{2+} adsorption by CH-SQ-25 beads

Kinetic model		Parameter	Heavy metal ion	
			Cu^{2+}	Zn^{2+}
Adsorption reaction[a]	Experimental	q_e (mg g^{-1})	40.1	8.3
	PFO[b]	q_e (mg g^{-1})	35.9	7.9
		R^2	0.7358	0.9371
	PSO[b]	q_e (mg g^{-1})	39.0	8.8
		R^2	0.9466	0.9733
Intraparticle diffusion[a]	Region 1 (30–90 min)	C_1 (mg g^{-1})	15.2	−0.5
		K_{IPD1} (mg g^{-1} min$^{-1/2}$)	1.53	0.65
		R^2	0.9941	0.9886
	Region 2 (90–360 min)	C_2 (mg g^{-1})	23.2	3.2
		K_{IPD2} (mg g^{-1} min$^{-1/2}$)	0.70	0.25
		R^2	0.9800	0.9640
	Region 3 (360–1440 min)	C_3 (mg g^{-1})	32.3	7.9
		K_{IPD3} (mg g^{-1} min$^{-1/2}$)	0.21	0.01
		R^2[c]	—	—

[a] For a solution concentration of 100 ppm. [b] Only parameters & correlation coefficients mentioned within the main text are displayed. The complete set of parameters are available as ESI. [c] R^2 was not calculated, as only two data points were fitted. However, it is assumed to be high due to the dataset representing the saturation/equilibrium region.

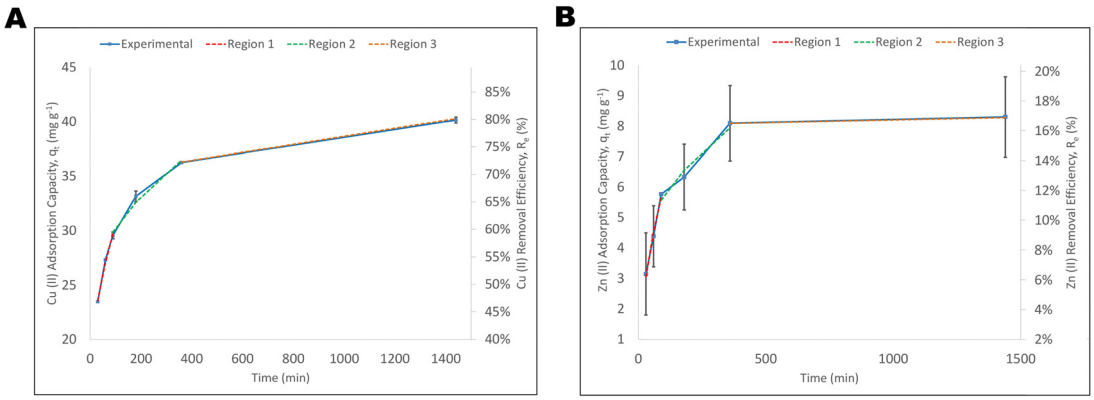

Fig. 6 Intraparticle diffusion (IPD) model in terms of adsorption capacity and removal efficiencies for the adsorption by CH-SQ-25 beads from 100 ppm heavy metal ion solutions – (A) Cu^{2+} and (B) Zn^{2+} – showing three independent regions: region 1 (30–90 min), region 2 (90–360 min), region 3 (360–1440 min).

25 beads, as indicated by lower rate constants.[56–59] Lastly, the third portion corresponds to an equilibrium stage, where IPD diffusion decelerates under the influence of low heavy metal ion concentration and possibly a transition to diffusion into micropores.[50,56,57,59] Considering the outlined multi-step process, mass transport likely depends on the concentration, size, bulk diffusion coefficient and biosorbent affinity of the heavy metal ion under consideration, as well as the pore-size distribution of the CH-SQ-25 beads.[56,59,60] Notably, the effect of heavy metal ion choice was clearly elucidated by the negative intercept for the initial region of Zn^{2+} adsorption, compared to the large positive intercept for Cu^{2+}. Similar phenomena have been reported in previous studies.[59,61] These were attributed to the combined effects of film diffusion and surface reaction control, indicating that chemisorption, which is usually faster than mass transfer, has a significant role in the rate-limiting step in the initial region of Zn^{2+} adsorption. This is consistent with the aforementioned lower affinity for Zn^{2+} compared to Cu^{2+}.

Equilibrium studies

The surface characteristics of CH-SQ-25 beads were elucidated through equilibrium adsorption studies. The Freundlich and Langmuir isotherms were employed to assess the distribution of heavy metal ions between the beads and the solution at equilibrium, with a 24-hour treatment period deemed suitable from kinetic studies. Analysis focused on the saturation of active sites due to excess heavy metal ions (*i.e.* high concentrations), with the isotherms enabling the determination of maximum adsorption capacities, q_m, for $Cu^{2+}$and Zn^{2+}, for comparison with previous work.

The equilibrium isotherm for Cu^{2+} adsorption by CH-SQ-25 beads was obtained for the concentration range of 50–250 ppm (Fig. 7(A)). The onset of active site saturation was observed. However, complete saturation was not achieved. Additionally, the correlation coefficients for the Langmuir and Freundlich isotherms were 0.9679 and 0.9769, respectively, indicating good accordance with the experimental data (Table 2).

The effect of initial solution concentration on Zn^{2+} uptake by CH-SQ-25 beads was investigated under identical conditions (Fig. 7(B)). Notably, a high degree of linearity suggested that the concentration range was insufficient to promote the saturation of active sites. As with Cu^{2+} adsorption, both the Langmuir and Freundlich isotherms demonstrated good accordance with the experimental data, as indicated by correlation coefficients of 0.9994 and 0.9959, respectively (Table 2).

The high correlation coefficients for both the Langmuir and Freundlich isotherms, in the case of both heavy metal ions, can be attributed to neither species achieving full saturation of the

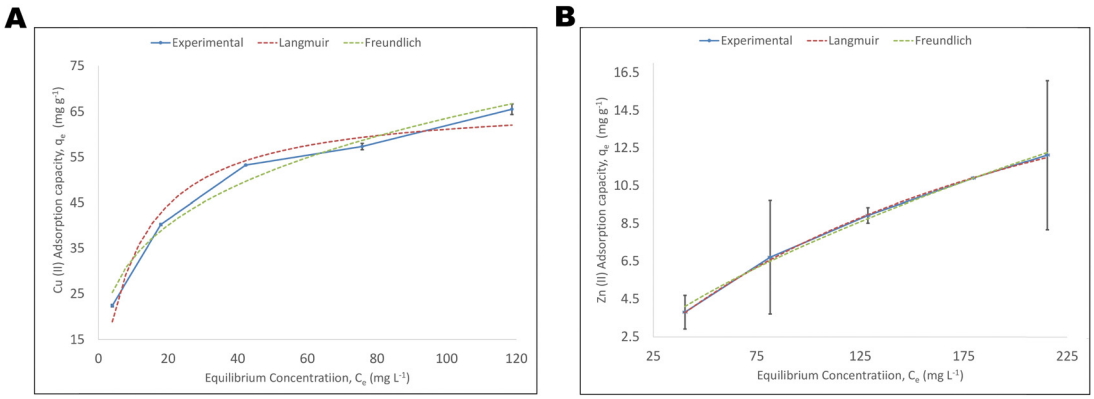

Fig. 7 Equilibrium isotherms for 24-hour treatment by CH-SQ-25 beads of heavy metal ion solutions: (A) Cu^{2+} and (B) Zn^{2+}.

Table 2 Equilibrium isotherm parameters for adsorption of Cu^{2+} and Zn^{2+} by CH-SQ-25 beads

Equilibrium isotherms	Parameter	Heavy metal ion	
		Cu^{2+}	Zn^{2+}
Langmuir[a]	q_m (mg g^{-1})	67.4	24.1
	R^2	0.9679	0.9994
	K_L (L mg^{-1})	0.0970	0.0046
	R_{L_U}[b]	0.171	0.813
	R_{L_L}[c]	0.040	0.465
Freundlich[a]	R^2	0.9769	0.9959

[a] Only parameters & correlation coefficients mentioned within the main text are displayed. The complete set of parameters are available as ESI. [b] R_{L_U} is the upper-limit Langmuir equilibrium parameter at 50 ppm. [c] R_{L_L} is the lower-limit Langmuir equilibrium parameter at 250 ppm.

CH-SQ-25 beads, as explained qualitatively in the preceding paragraphs. This indicates that the concentration range was too narrow, covering only the phase corresponding to relatively low heavy metal ion concentrations, where both models accurately account for partial adsorbent coverage and occupation of available sites. The findings may also be explained by Henry's law not being satisfied over the low concentration range, which results in the collapse of the Freundlich isotherm.[50] Intuitively, this suggest that adsorption was limited to monolayer coverage since the concentration range was inadequately low to support multilayer coverage. Thus, the Langmuir isotherm was selected as the more appropriate model, suggesting that Cu^{2+} and Zn^{2+} adsorption by CH-SQ-25 beads occurs *via* monolayer coverage of homogeneous active sites, with negligible interactions among the adsorbed heavy metal ions.[15,28] The decisions is further supported by the prevalence of the Langmuir isotherm in literature to describe the uptake of Cu^{2+} and Zn^{2+} by chitosan-based biosorbents beads.[15,22,46,54,62–65] Importantly, while the adoption of the Freundlich isotherm has been limited, several of these studies have also reported high correlation coefficients for the model, with some of the results being subject to similar criticism due to the use of inadequately narrow concentration ranges.[22,47,54,66]

Based on the Langmuir isotherm, the CH-SQ-25 beads had a maximum adsorption capacity of 67.4 and 24.1 mg g^{-1} for Cu^{2+} and Zn^{2+}, respectively (Table 2). These values confirmed that the concentration range was inadequately low since the studies only achieved adsorption capacities of 65.5 and 12.1 mg g^{-1} for Cu^{2+} and Zn^{2+}, respectively. In fact, only 50% of the maximum adsorption capacity for Zn^{2+} was achieved. To experimentally validate the maximum adsorption capacities for both Cu^{2+} and Zn^{2+}, higher concentrations should be studied to achieve near complete saturation of active sites and full monolayer coverage.

The lower affinity of CH-SQ-25 beads for Zn^{2+} was supported by a lower maximum adsorption capacity compared to the value for Cu^{2+}. This observation was consistent with previous studies. The Langmuir constant, K_L, provided additional evidence of the lower affinity for Zn^{2+} (Table 2). In this regard, the much large K_L value for Cu^{2+} (0.0970 L mg^{-1}), compared to the value for Zn^{2+} (0.0046 L mg^{-1}), indicated a much stronger binding affinity. Further elucidation of the lower affinity of CH-SQ-25 beads for Zn^{2+} was provided by the Langmuir equilibrium parameters, R_L, for which lower values within the range of 0–1 indicate more favourable adsorption. In this regard, the R_L values for Zn^{2+} exceeded 0.4 over the entire initial concentration range while those for Cu^{2+} were consistently lower than 0.2. Regardless, the adsorption of both heavy metal ions was favourable. Notably, the lower affinity for Zn^{2+} has previously been attributed to the higher stability of Cu^{2+} complexes on the William–Irving series.

Lastly, CH-SQ-25 beads exhibited competitive performance compared to other chitosan-based beads reported in literature (Table 3). Appreciable improvements for the adsorption of Zn^{2+} and Cu^{2+} compared to other crosslinked hydrogel beads were reported. Only conventional grafting yielded chitosan-based biosorbents possessing maximum adsorption capacities that surpassed those of CH-SQ-25 beads. This finding highlighted the effectiveness of IL treatment using [BMIM][OAc] as a highly convenient functionalization method, which can compensate for losses in adsorption capacity from crosslinking without requiring the complexity associated with conventional grafting.

Sustainability metrics

The promotion of green chemistry in the synthesis of chitosan-based adsorbents by recasting from [BMIM][OAc] was assessed. Atom economy and E-factor were employed. The calculations focused solely on the CH bead type due to the certainty of functional groups on β-chitosan with 92% deacetylation and molecular weight of approximately 580 000 da.

Atom economy considered crosslinking with glutaraldehyde by imine bond formation, involving condensation reactions. A conservative value of 91.61% was obtained assuming complete saturation of amine sites. However, this scenario was unlikely due to the participation of free amine sites in the adsorption of heavy metal ions. The actual atom economy has been projected between 91.61–100%.

The E-factor considered the recyclability of [BMIM][OAc], DMSO and absolute ethanol, as well as the full recovery of β-chitosan in the CH beads. Losses solely considered the spent glutaraldehyde solution. An optimal estimate of 0.105 was noted for the retention of glutaraldehyde corresponding to complete saturation of amine sites. However, acknowledging the non-crosslinked amine sites, a conservative estimate was obtained under the assumption of no crosslinking and the loss of all glutaraldehyde solution. The actual E-factor has been projected between 0.105–0.441.

The preparation of chitosan-based beads by IL treatment in [BMIM][OAc] exhibited excellent atom economy and low E-factor. Furthermore, using SP protein as a co-polymer affords additional merit by decreasing the environmental footprint and overall cost of the biosorbents, given that β-chitosan is much more costly due to the resource intensiveness of its synthesis.

Conclusions

Biosorbent beads for heavy metal ion removal from wastewater were successfully prepared from β-chitosan and SP protein, by

Table 3 Preparation methodology, equilibrium batch study conditions, and maximum adsorption capacities (mg g^{-1}) of chitosan-based biosorbent beads from literature

Modification type	Specific preparation method	Sol. pH	Conc. range (ppm)	Equilibrium time (h)	Adsorbent mass (g)	Sol. volume (mL)	Max. adsorption capacity (mg g^{-1}) Cu^{2+}	Max. adsorption capacity (mg g^{-1}) Zn^{2+}	Authors
Crosslinking	Sodium tripolyphosphate	4.5	20–300	1.66	0.20	50	26.06	—	Wan Ngah & Fatinathan[50]
Crosslinking	Glutaraldehyde	6.0	0–14	1.00	0.01	100	59.67	—	Wan Ngah *et al.*[65]
	Epichlorohydrin	6.0	0–14	1.00	0.01	100	62.47	—	
	Ethylene glycol diglycidyl ether	6.0	0–14	1.50	0.01	100	45.62	—	
Crosslinking	Epichlorohydrin	6.0	0–15	4.00	0.01	100	35.46	10.21	Chen *et al.*[64]
IL treatment, IPN	Chitosan–cellulose (1 : 2) from [EMIM][Cl]	—	32–2500	24.00	0.25	10	36.03	3.45	Matsumoto *et al.*[54]
IL treatment, IPN	Chitosan–cellulose (1 : 2) from [BMIM][Cl]	5.8	—	10	0.1	50	26.46	19.81	Sun. *et al.*[19]
IL treatment, IPN	Chitosan–cellulose (1 : 3) from [BMIM][OAc]	—	50–250	48.00	0.5	20	26.70	—	Wittmar *et al.*[22]
IL treatment, IPN	Chitosan–cellulose (1 : 3) from [EMIM][OAc]	—	50–250	48.00	0.5	20	15.80	—	
Grafting	Polyaniline	5.0	40–400	2.50	0.45	100	83.3	—	Igberase *et al.*[15]
Grafting	Enediaminetetraacetic acid	—	10–200	24.00	0.01	10	31.64	24.27	Karimi *et al.*[62]
Crosslinking, grafting	Epichlorohydrin, 4-aminobenzoic acid	5.0[a] 7.0[b]	40–160	1.00	0.008	100	140.5	130.6	Igberase *et al.*[63]
Crosslinking, grafting	Epichlorohydrin, 8-hydroxyquinoline	5.0	80–1000[a] 10–200[b]	24.00	0.10	10	52.9	8.203	Barros *et al.*[66]
Crosslinking, grafting	Glutaraldehyde, methacrylamide	5.0	200–600	5.00	0.10	20	140.9	—	Sutirman *et al.*[46]
IL treatment, IPN, crosslinking	CH-SQ-25 beads	5.0[a] 6.0[b]	50–250	24.00	0.025	12	67.4	24.1	This Study

[a] Experimental conditions and parameters used exclusively for Cu^{2+} studies. [b] Experimental conditions and parameters used exclusively for Zn^{2+} studies.

regeneration from [BMIM][OAc]. The physical, functional and adsorptive properties of the hybrid biosorbents beads were investigated to assess the contributions of SP protein.

Physical characterisation uncovered increased brittleness at higher SP protein content in CH-SQ-25 and CH-SQ-50 beads. Additionally, observable brittleness of CH beads suggested that IL treatment with [BMIM][OAc] and glutaraldehyde crosslinking also contributed to fragility, highlighting the need for optimizing the preparation process. In this context, the extrusion stage was identified as particularly significant, as the current methodology may have been better suited for hydrogel beads with lower SP protein content and more viscous casting solutions. Notably, all bead types exhibited fibrous and porous structures. However, additional studies employing BET analysis and scanning electron microscopy (SEM) are recommended for examining the effect of SP protein content on the internal polymer network, specific surface area, pore-size distribution and surface morphology.

FT-IR analysis revealed that IL regeneration enhances the functional group availability on chitosan. However, SP protein was noted to diminish β-chitosan's characteristic bands. Given a relationship between FT-IR intensity and co-polymer dosage, X-ray photoelectron spectroscopy (XPS) may be used for the analysis of specific functional groups, such as N-containing groups. Alternatively, titration may be adopted for quantitative analysis of active functional groups.

Adsorption studies highlighted less efficient heavy metal ion removal at lower pH levels, with adsorption being optimal at pH 5 and 6 for Cu^{2+} and Zn^{2+}, respectively. Concerning SP protein, it was observed that higher contents corresponded to a decrease in the removal efficiency of Cu^{2+} and Zn^{2+}. Additionally, reaction kinetic studies with CH-SQ-25 beads showed rapid adsorption of Cu^{2+} and Zn^{2+}, following pseudo-second-order kinetics, which is indicative of chemisorption. Regarding mass transfer, a multi-step process was observed, with the transport of Cu^{2+} and Zn^{2+} to the adsorbent sites being successively controlled by external diffusion, intraparticle diffusion and equilibrium over distinct time periods. Lastly, equilibrium studies based on the Langmuir isotherm indicated that CH-SQ-25 beads have higher maximum adsorption capacities for Cu^{2+} and Zn^{2+} than similar hydrogel beads reported in literature. Notably, investigations should be conducted with competitive multi-metal solutions and samples of industrial effluents, to assess the performance and selectivity of the CH-SQ-25 beads under more representative conditions. Desorption studies, conducted over several adsorption cycles, are also important for verifying the reusability of the CH-SQ-25 beads and examining potential efficiency loss. Lastly, further studies on multifarious heavy metal solutions should consider anionic coordination compounds, to elucidate the influence of the higher cationic surface charge of SP protein.

The inclusion of SP protein did not improve the heavy metal adsorption capability of β-chitosan. However, its inclusion as a cost-reducing filler may be suggested considering the chemical stability, rapid adsorption kinetics, high adsorption capacity and improved sustainability of the synthesized biosorbent beads. Moreover, optimization of the preparation process holds vast potential for enhancing the mechanical integrity and

uniformity of hybrid β-chitosan-SP protein biosorbent beads. Beyond this, the proof of concept for IL treatment in preparing highly porous and functionalized β-chitosan-based materials can be extended to other co-polymer blends, which may demonstrate additional merit for large-scale wastewater treatment.

Data availability

The data supporting this article have been included as part of the ESI.†

Conflicts of interest

There are no conflicts to declare.

Acknowledgements

The research reported here was funded by the Commonwealth Scholarship Commission and the Foreign, Commonwealth and Development Office in the UK. I am grateful for their support. All views expressed here are those of the author(s) not the funding body. PYSN and JH are also grateful to the UKRI for support through the Supergen Bioenergy Impact Hub 2023 (EP/Y016300/1).

References

1 S. K. Gunatilake, *J. Multidiscip. Eng. Sci.*, 2015, **1**, 12–18.
2 R. Verma and P. Dwivedi, *Recent Res. Sci. Technol.*, 2013, **5**, 98–99.
3 S. Sarode, P. Upadhyay, M. A. Khosa, T. Mak, A. Shakir, S. Song and A. Ullah, *Int. J. Biol. Macromol.*, 2019, **121**, 1086–1100.
4 R. Bisht, M. Agarwal and K. Singh, *J. Water Reuse Desalin.*, 2017, **7**, 387–419.
5 N. A. A. Qasem, R. H. Mohammed and D. U. Lawal, *npj Clean Water*, 2021, **4**, 36.
6 X. Xie, C. Chen, N. Zhang, Z.-R. Tang, J. Jiang and Y.-J. Xu, *Nat. Sustain.*, 2019, **2**, 856–864.
7 Z. Liu, Z. Xu, L. Xu, F. Buyong, T. C. Chay, Z. Li, Y. Cai, B. Hu, Y. Zhu and X. Wang, *Carbon Res.*, 2022, **1**, 8.
8 S. Das, S. R. Paul and A. Debnath, *J. Mol. Liq.*, 2023, **387**, 122610.
9 L. Wang, Y. Wang, F. Ma, V. Tankpa, S. Bai, X. Guo and X. Wang, *Sci. Total Environ.*, 2019, **668**, 1298–1309.
10 F. S. Nworie, N. Mgbemena, A. C. Ike-Amadi and J. Ebunoha, *J. Hum. Earth, Future*, 2022, **3**, 377–395.
11 K. H. Carrasco, E. G. Höfgen, D. Brunner, K. B. L. Borchert, B. Reis, C. Steinbach, M. Mayer, S. Schwarz, K. Glas and D. Schwarz, *Polysaccharides*, 2022, **3**, 356–379.
12 L. A. M. Van Den Broek and C. G. Boeriu, *Chitin and Chitosan: Properties and Applications*, John Wiley & Sons, Hoboken, NJ, 2020.
13 E. S. Abdou, K. S. A. Nagy and M. Z. Elsabee, *Bioresour. Technol.*, 2008, **99**, 1359–1367.
14 B. Qu and Y. Luo, *Int. J. Biol. Macromol.*, 2020, **152**, 437–448.
15 E. Igberase, P. Osifo and A. Ofomaja, *J. Environ. Chem. Eng.*, 2014, **2**, 362–369.
16 D. Kong, S. R. Foley and L. D. Wilson, *Molecules*, 2022, **27**, 978.
17 J. Gomez-Pastora, E. Bringas and I. Ortiz, *Chem. Eng. J.*, 2014, **256**, 187–204.
18 S. Das, A. Pal and A. Debnath, *ChemistrySelect*, 2023, **8**, e202300928.
19 X. Sun, B. Peng, Y. Ji, J. Chen and D. Li, *AIchE J.*, 2009, **55**, 2062–2069.
20 Q. Chen, A. Xu, Z. Li, J. Wang and S. Zhang, *Green Chem.*, 2011, **13**, 3446–3452.
21 S.-T. Lee, F.-L. Mi, Y.-J. Shen and S.-S. Shyu, *Polymer*, 2001, **42**, 1879–1892.
22 A. S. M. Wittmar, H. Bohler, A. L. Kayali and M. Ulbricht, *Cellulose*, 2020, **27**, 5689–5705.
23 I. O. Saheed and F. B. M. Suah, *Int. J. Biol. Macromol.*, 2023, **241**, 124610.
24 E. S. Dragan, *Chem. Eng. J.*, 2014, **243**, 572–590.
25 T. Albrecht, J. Addai-Mensah and D. Fornasiero, Effect of pH, concentration and temperature on copper and zinc hydroxide formation/precipitation in solution, in *Chemeca 2011: Engineering a Better World: Sydney Hilton Hotel, NSW, Australia, 18–21 September 2011*, Engineers Australia, Barton, A.C.T., 2011, pp. 2100–2110.
26 N. Farnad, N. H. Voelcker and K. Farhadi, *Water, Air, Soil Pollut.*, 2012, **223**, 3535–3544.
27 G. Karthikeyan, K. Anbalagan and N. Muthulakshmi Andal, *J. Chem. Sci.*, 2004, **116**, 119–127.
28 Z. A. Sutirman, M. M. Sanagi, K. J. Abd Karim and W. A. Wan Ibrahim, *Carbohydr. Polym.*, 2016, **151**, 1091–1099.
29 S. Maseldzija, J. Petrovic, A. Onjia, T. Volkov-Husovic, A. Nesic and N. Vukelic, *J. Ind. Eng. Chem.*, 2019, **75**, 246–252.
30 S. Hojati and A. Landi, *Int. J. Environ. Sci. Technol.*, 2015, **12**, 203–210.
31 R. Fernandez-Gonzalez, M. A. Martín-Lara, J. A. Moreno, G. Blazquez and M. Calero, *J. Cleaner Prod.*, 2019, **227**, 634–644.
32 C. A. Basha, S. J. Selvi, E. Ramasamy and S. Chellammal, *Chem. Eng. J.*, 2008, **141**, 89–98.
33 M. Sciban, B. Radetic, Z. Kevresan and M. Klasnja, *Bioresour. Technol.*, 2007, **98**, 402–409.
34 H. Xu, D.-D. Liu, L. He, N. Liu and G. Ning, *Iran J. Chem. Chem. Eng.*, 2015, **34**, 73–81.
35 K. Dermentzis, A. Christoforidis and E. Valsamidou, *Int. J. Environ. Sci.*, 2019, **5**, 21–34.
36 C.-G. Lee, S. Lee, J.-A. Park, C. Park, S. J. Lee, S.-B. Kim, B. An, S.-T. Yun, S.-H. Lee and J.-W. Choi, *Chemosphere*, 2017, **166**, 203–211.
37 V. Stankovic, D. Bozic, M. Gorgieviski and G. Bogdanovic, *Chem. Ind. Chem. Eng. Q.*, 2009, **15**, 237–249.

38 S. Miličević, M. Vlahovic, M. Kragovic, S. Martinovic, V. Milosevic, I. Jovanovic and M. Stojmenovic, *Minerals*, 2020, **10**, 753.
39 G. T. George and J. J. Gabriel, *Haya: Saudi J. Life Sci.*, 2017, **2**, 108–115.
40 M. B. Desta, *J. Thermodyn.*, 2013, **2013**, 375830.
41 I. Bencheikh, K. Azoulay, J. Mabrouki, S. El Hajjaji, A. Moufti and N. Labjar, *Chem. Data Collect.*, 2021, **31**, 100597.
42 M. Aleem, J. Cao, C. Li, H. Rashid, Y. Wu, M. I. Nawaz, M. Abbas and M. W. Akram, *Water, Air, Soil Pollut.*, 2020, **231**, 45.
43 E. F. Sharaf and E. Alharbi, *Afr. J. Biotechnol.*, 2013, **12**, 4351–4355.
44 N. F. Fahim, B. N. Barsoum, A. E. Eid and M. S. Khali, *J. Hazard. Mater.*, 2006, **B136**, 303–309.
45 N. Sooksawat, M. Meetam, M. Kruatrachue, P. Pkethitiyook and D. Inthorn, *Biorem. J.*, 2016, **20**, 240–251.
46 Z. A. Sutirman, M. M. Sanagi, K. J. Abd Karim, W. A. Wan Ibrahim and B. H. Jume, *Int. J. Biol. Macromol.*, 2018, **116**, 255–263.
47 W. S. Wan Ngah and S. Fatinathan, *Chem. Eng. J.*, 2008, **143**, 62–67.
48 S. Islam, L. Arnold and R. Padhye, *BioMed Res. Int.*, 2015, **2015**, 874316.
49 A. Shanmugapriya, A. Srividhya, R. Ramya and P. N. Sudha, *Int. J. Environ. Sci.*, 2011, **1**, 2086–2095.
50 W. S. Wan Ngah and S. Fatinathan, *J. Environ. Manage.*, 2010, **91**, 958–969.
51 N. Li and R. Bai, *Ind. Eng. Chem. Res.*, 2005, **44**, 6692–6700.
52 A. Barth, *Biochim. Biophys. Acta, Bioenerg.*, 2007, **1767**, 1073–1101.
53 S. A. Dharaskar, M. N. Varma, D. Z. Shende, C. Kyoo Yoo and K. L. Wasewar, *Sci. World. J.*, 2013, **2013**, 395274.
54 M. Matsumoto, S. Ishikawa and T. Kamigaki, *Prog. Chem. Appl. Chitin Its Deriv.*, 2019, **24**, 145–150.
55 A. Miličević, G. Branica and N. Raos, *Molecules*, 2011, **16**, 1103–1112.
56 W. H. Cheung, Y. S. Szeto and G. McKay, *Bioresour. Technol.*, 2006, **98**, 2897–2904.
57 M. Benavente, L. Moreno and J. Martinez, *J. Taiwan Inst. Chem. Eng.*, 2011, **42**, 976–988.
58 I. Tsibranska and E. Hristova, *Bulg. Chem. Commun.*, 2011, **43**, 370–377.
59 K. L. Tan and B. H. Hameed, *J. Taiwan Inst. Chem. Eng.*, 2017, **74**, 25–48.
60 F.-C. Wu, R.-L. Tseng and R.-S. Juang, *Chem. Eng. J.*, 2009, **153**, 1–8.
61 P. A. Kotabwatta, L. B. L. Lim and N. Priyantha, *Ceylon J. Sci., Biol*, 2023, **52**, 71–81.
62 F. Karimi, A. Ayati, B. Tanhaei, A. L. Sanati, S. Afshar, A. Kardan, Z. Dabirifar and C. Karaman, *Environ. Res.*, 2022, **203**, 111753.
63 E. Igberase, A. Ofomaja and P. O. Osifo, *Int. J. Biol. Macromol.*, 2019, **123**, 664–676.
64 A.-H. Chen, S.-C. Liu, C.-Y. Chen and C.-Y. Chen, *J. Hazard. Mater.*, 2008, **154**, 184–191.
65 W. S. Wan Ngah, C. S. Endud and R. Mayanar, *React. Funct. Polym.*, 2002, **50**, 181–190.
66 F. C. F. Barros, F. W. Sousa, R. M. Cavalcante, T. V. Carvalho, F. S. Dias, D. C. Queiroz, L. C. G. Vasconcellos and R. F. Nascimento, Removal of Copper, Nickel and Zinc Ions from Aqueous Solution by Chitosan-8-Hydroxyquinoline Beads, *Clean-Soil Air Water*, 2008, **36**, 292–298.

